

# Train a Real-world Local Path Planner in One Hour via Partially Decoupled Reinforcement Learning and Vectorized Diversity

Jinghao Xin<sup>a</sup>, Jinwoo Kim<sup>b</sup>, Zhi Li<sup>a</sup>, Ning Li<sup>a,\*</sup>

<sup>a</sup>Department of Automation, Shanghai Jiao Tong University, Shanghai 200240, P.R. China

<sup>b</sup>School of Civil and Environmental Engineering, Nanyang Technological University, S639798, Singapore

## Abstract

Deep Reinforcement Learning (DRL) has exhibited efficacy in resolving the Local Path Planning (LPP) problem. However, such application in the real world is immensely limited due to the deficient training efficiency and generalization capability of DRL. To alleviate these two issues, a solution named Color is proposed, which consists of an Actor-Sharer-Learner (ASL) training framework and a mobile robot-oriented simulator Sparrow. Specifically, the ASL intends to improve the training efficiency of DRL algorithms. It employs a Vectorized Data Collection (VDC) mode to expedite data acquisition, decouples the data collection from model optimization by multithreading, and partially connects the two procedures by harnessing a Time Feedback Mechanism (TFM) to evade data underuse or overuse. Meanwhile, the Sparrow simulator utilizes a 2D grid-based world, simplified kinematics, and conversion-free data flow to achieve a lightweight design. The lightness facilitates vectorized diversity, allowing diversified simulation setups across extensive copies of the vectorized environments, resulting in a notable enhancement in the generalization capability of the DRL algorithm being trained. Comprehensive experiments, comprising 57 DRL benchmark environments, 32 simulated and 36 real-world LPP scenarios, have been conducted to corroborate the superiority of our method in terms of efficiency and generalization. The code and the video of this paper are accessible at <https://github.com/XinJingHao/Color>.

**Keywords:** Deep reinforcement learning, Local path planning, Mobile robot, Sim2Real

## 1. Introduction

Local path planning portrays a pivotal role in the autonomous navigation of mobile robots, endowing them with the capability to execute unmanned missions such as disaster rescue, military reconnaissance, and material distribution. Given the static path generated by the global path planning algorithm, the LPP yields a collision-free path in accordance with certain metrics to circumvent the newly arisen obstacles while navigating. Traditional LPP approaches, such as Dynamic Window Approach [1] and Fuzzy Logic Algorithm [2], predominantly rely on expert knowledge to deliberately engineer their parameters. Nonetheless, these handcrafted fixed parameters can incur performance deterioration when confronted with complex environments [3, 4].

Deep Reinforcement Learning (DRL) is promising to alleviate the aforementioned issue. In DRL, the agent learns by interacting with the environment and is capable of attaining human-level decision-making and control performance. To date, DRL has made remarkable strides in fields such as video games [5], chess [6], navigation [7], and ChatGPT [8]. Nevertheless, despite these momentous breakthroughs, the applications of DRL have been predominantly restricted to the virtual or simulated

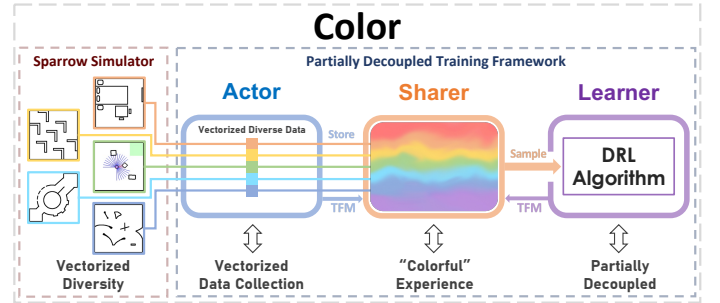


**Fig. 1.** An overview of Color. The left part is the mobile robot-oriented simulator Sparrow, where simulation parameters (such as control interval, control delay, fraction, inertia, velocity range, and sensor noise) and training maps can be readily diversified via vectorized environments. The right part illustrates our efficient DRL training framework, ASL. The seamless integration between Sparrow and ASL is achieved through their interdependent vectorized environments. Notably, Color exhibits the capability to rapidly train a DRL-based local path planner with high generalization capacity.

world. The disappointing efficiency and generalization of DRL have formed a longstanding impediment to its real-world applications. (1) *Sample efficiency*: the training of the DRL agent is exceptionally demanding in terms of training samples, which can be prohibitively costly to collect in the real world. (2) *Training time efficiency*: it could consume days or even weeks to train a desirable DRL agent in complex environments. (3) *Simulation to real world generalization (Sim2Real)*: to sidestep the unacceptable training time in the real world, researchers

\*Corresponding author

Email addresses: xjhzsj2019@sjtu.edu.cn (Jinghao Xin), jinwoo.kim@ntu.edu.sg (Jinwoo Kim), lizhibeaman@sjtu.edu.cn (Zhi Li), ning\_li@sjtu.edu.cn (Ning Li)

typically resort to accelerated physics simulation platforms, with the expectation that the model trained in a simulator can be transferred to real-world situations. However, the discrepancy between the simulated and the real world is challenging to diminish, thus significantly impeding the transfer. (4) *Task to Task generalization (Task2Task)*: the DRL agent is prone to overfit to the training environments, resulting in performance degeneration as the environment changes. Consequently, ameliorating the efficiency and generalization of DRL is challenging but advantageous, which constitutes the overarching purpose of this research. The main contributions of this paper can be drawn as follows.

- 1) A partially decoupled training framework, namely Actor-Sharer-Learner (ASL), is proposed to improve the training efficiency of the DRL algorithm. Experiments demonstrate that mainstream off-policy DRL algorithms with experience replay can be readily integrated into our framework to enjoy a remarkable promotion.
- 2) A lightweight mobile robot-oriented simulator named Sparrow has been developed. The lightness of Sparrow boosts its vectorization, which not only expedites data generation but also enables vectorized diversity, allowing diverse simulation setups across different copies of the vectorized environments to enhance the generalization of the trained DRL algorithms.
- 3) Combining the ASL with Sparrow through their interdependent vectorized environments, we formulate our DRL solution to the LPP problem, referred to as Color. Through one hour of simulation training, the Color is capable of yielding a real-world local path planner with laudable resilience to generalize over a wide variety of scenarios.

The remainder of this paper is organized as follows. Related works concerning DRL’s efficiency, generalization, and commonly used simulators are reviewed in Section 2. The ASL training framework and the Sparrow simulator are introduced in Section 3. Comprehensive experiments involving the evaluation of ASL, Sparrow, and the trained local path planner have been conducted in Section 4. The conclusion is derived in Section 5.

## 2. Related works

This section reviews related works that aim to enhance the efficiency and generalizability of DRL algorithms, as well as the simulation platforms commonly utilized in DRL.

### 2.1. Efficiency of DRL

The prevalence of DRL has been severely bottlenecked by its unsatisfactory sample efficiency. To mitigate this issue, numerous methods have been proposed. From the perspective of model architecture, Wang *et al.* [9] integrated the dueling network into the DRL. The dueling network enables information generalizing across actions, thus reducing the samples needed for training. Fortunato *et al.* [10] injected the DRL model with learnable random variables such that the derived model

could yield state-dependent, consistent exploration strategies so as to generate high-quality data that facilitate training. From the perspective of sample utilization, Schaul *et al.* [11] devised the Prioritized Experience Replay (PER). In contrast to uniformly sampling from past experiences, PER samples experiences in accordance with their respective TD-error. The TD-error mirrors how “surprising” one experience is, thus prompting the agent to focus on the instrumental samples. However, the PER may lead to data overuse or even model collapse. To tackle this issue, Wei *et al.* [12] augmented the TD-error with a quantum-inspired representation to ensure the diversity of the replayed experiences. One common drawback of the aforementioned methods is that the training procedure is pended during the agent’s interaction with the environment. This alternation between model optimization and data collection results in low training time efficiency.

To elevate the training time efficiency of DRL, Mnih *et al.* [13] proposed the Asynchronous Advantage Actor-Critic (A3C) framework. With the aid of distributed data collection and asynchronous model optimization, A3C remarkably shortens the training time versus the standard DRL method. However, the training data in A3C is discarded immediately once the gradients have been computed, giving rise to its low sample efficiency. Contrastingly, the Ape-X [14] framework employed a shared memory to store the experiences generated by these distributed agents and optimized the model in an off-policy manner so that the experiences could be reused. Analogously to A3C, the Ape-X decoupled the data collection and model optimization procedures into multi-actor and one learner, then ran them concurrently to improve training time efficiency. Nevertheless, there are two notable drawbacks in the Ape-X framework. First, the multi-thread deployed actor mode is inefficient, which could exert three adverse repercussions upon the learning system: a) if the Forward Propagation (FP) of the network is computed by the CPU, it precludes the usage of large-scale networks because the CPU is notorious for its inefficiency in large scale networks computing. b) if the FP is computed by the GPU, the parallel computing feature of the GPU is not fully utilized, for the computation is requested separately and asynchronously by actors. c) the data flow in Ape-X is cumbersome and could be bottlenecked by the transmission bandwidth, where the data is firstly accumulated by the local buffer of each actor and then packed into the shared memory by a background thread. Second, the actors and learner are completely decoupled without coordinating their running speeds. If actors run far slower than the learner, it’s likely that the data is overused, which could adversely impact its stability. Otherwise, the data might be abandoned without full utilization, resulting in low sample efficiency. In the experiments of [14], despite being equipped with dueling networks and PER to enhance its sample efficiency, Ape-X requires a hundred times more samples to surpass other DRL baselines. Since the relative speed of the actors and learner can be influenced by the breakdown of actors or fluctuates with the hardware occupation [14], these two unfavorable cases are inevitable. Hence, further works need to be done to resolve the shortcomings of existing research.

## 2.2. Generalization of DRL

Methods concerning improving the Sim2Real generalization primarily involve three categories. (1) System identification [15]: define and tune the parameters to match the real-world environment. (2) Domain Randomization (DR) [16]: randomize the simulation setups while training such that the real-world environment can be deemed as another variation of these randomized environments. (3) Domain adaptation [17, 18]: adapt the trained model by learning mapping or invariant features from simulation to the real world, or re-training in the real world. Regarding Task2Task generalization, the methodologies mainly encompass four classifications. (1) Employing apposite task description: RMDP [19] and MOO-MDP [20]. (2) Introducing diversity: randomly generated visual properties [21], randomly initialized agent and environment [22]. (3) Data augmentation: image processing techniques [23], automatic data augmentation [24], and random convolution [25]. (4) Regularization [26]: L2-regularization, dropout, and batch normalization. Although a wide range of studies has been carried out on the generalization of DRL, their focuses, however, are limited to the standard DRL framework. The combination of such techniques with high-efficient training frameworks, such as decoupled framework, has not been carefully discussed, which we believe is indispensable and could be a desirable incentive to the wide-ranging application of DRL.

## 2.3. Simulation platform

Gazebo [27] is a 3D physics-based robotic simulation platform and has been wildly employed in various robotic systems, such as Automated Guided Vehicles (AGVs) [22], manipulators [28], and Unmanned Aerial Vehicles (UAVs) [29]. Nonetheless, the Gazebo is demanding in computational resources due to the complicated physics calculation, which results in low simulation speed and considerably impairs the efficiency of the trained DRL algorithm [30, 31, 32]. CoinRun [26] and Procgen [21] are two simulators that intend to ameliorate the generalization dilemma of the DRL agent by providing procedurally-generated visual diversity. Regrettably, it must be noted that CoinRun and Procgen are specifically designed for video games and lack support for physics simulation. As a result, they are unable to contribute to improving the generalization capabilities of agents confronting real-world applications.

## 3. Methodology

In this section, we will first elaborate on our efficient training framework and our mobile robot-oriented simulator, and then discuss how to elegantly combine them together, fully taking their respective advantage, to form the DRL solution to LPP problems, namely the Color.

### 3.1. Actor-Sharer-Learner training framework

The Related Works concerning the efficiency of DRL reveal a contradiction between sample efficiency and training time efficiency. Despite extensive efforts to tackle these challenges, existing approaches remain separate. We argue that both the

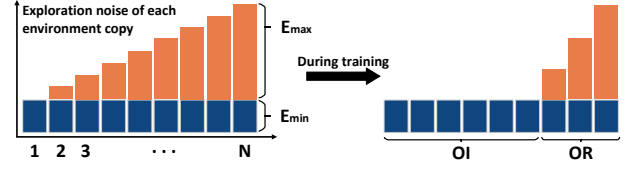


**Fig. 2.** Vectorized  $\epsilon$ -greedy Exploration Mechanism. Here, the horizontal axis is the index of the vectorized environments, and  $N$  is the total number of vectorized environments.

sample and training time efficiency are prominent for DRL, and improving them simultaneously could considerably boost the application of DRL. In pursuit of this goal, we proposed the ASL training framework.

To equip our framework with high training time efficiency, we inherit the decoupled architecture from Ape-X. As shown in Fig. 3, an actor and a learner are employed to collect data and optimize the model individually. The actor and learner run concurrently in different threads, and the information that needs to be shared is managed by a sharer. As aforementioned, the Ape-X is sorely restricted by its multi-thread deployed actor mode and completely decoupled architecture. We tackle the first issue by resorting to the vectorized environments [33] and the second issue by adding a Time Feedback Mechanism (TFM) between the actor and the learner.

#### 3.1.1. Vectorized data collection

The vectorized environments runs multiple copies of the same environment parallelly and independently, interacting with the actor in a batched fashion. The superiority of vectorized environments is evidently. First, the vectorized environments interacts with the actor in a batched way such that the parallel computation advantage of GPU could be exploited to the fullest extent. Second, when interacting with vectorized environments of  $N$  copies, the VDC mode necessitates only a single instantiation of the actor network due to the batched interaction, leading to a substantial reduction in hardware resource requirements in contrast to the multi-thread deployed actor mode that requires  $N$  instantiations. Third, the batched data is stored as a whole in the experience buffer, eliminating the need for the thread lock stemming from asynchronous data preservation requests caused by multiple actors. Accordingly, it is reasonable to imagine that the three merits could additionally shorten the time needed for training.

Correspondingly, a Vectorized  $\epsilon$ -greedy Exploration Mechanism (VEM) is devised. In canonical  $\epsilon$ -greedy exploration, the agent executes its own policy at a probability of  $1 - \epsilon$  and explores the environment at a probability of  $\epsilon$ . The exploration noise  $\epsilon$  is linearly or exponentially decreasing during training. Although the  $\epsilon$ -greedy exploration is promising to maintain a balance between exploitation and exploration, its limitation is self-evident. The exploration is only guaranteed at the beginning of training and is eventually replaced with exploitation due to the decreasing noise. We argue this setting can be irrational in some contexts, especially when the environment is non-stationary. For instance, in some video games, the agent

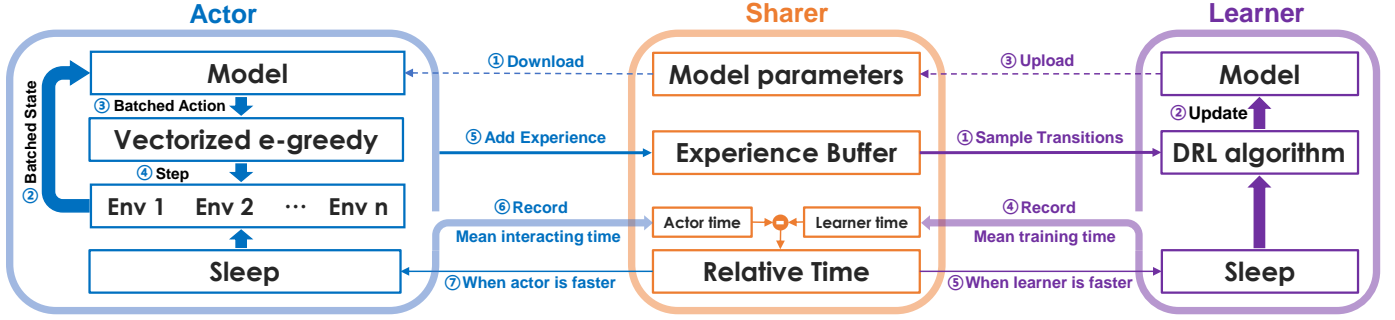


Fig. 3. Schematic of the Actor-Sharer-Learner training framework

#### Algorithm 1: Actor

---

Initialize the maximal interaction steps to  $T$ , vectorized environments (envs) with  $N$  copies, and total steps  $T_{step} = 0$   
 $s = \text{envs.reset}()$  // Generate the initial batched state  
**while**  $T_{step} < T$  **do**  
  1.  $\theta_a \leftarrow \theta_s$  // Inquire the Sharer whether there is a new model to download.  
  2.  $\mathbf{a} = \pi(\mathbf{s}; \theta_a)$  // Map the batched state to batched action with the latest policy  $\pi(\theta_a)$ .  
  3.  $\hat{\mathbf{a}} = \text{VEM}(\mathbf{a})$  // Inject the batched action with stochastic action by the VEM.  
  4.  $\mathbf{s}', \mathbf{r}, \text{done} = \text{envs.step}(\hat{\mathbf{a}})$   
  5.  $\text{Sharer.buffer.add}(\mathbf{s}, \hat{\mathbf{a}}, \mathbf{r}, \mathbf{s}', \text{done})$  // Add the batched transitions to Sharer.  
  6.  $V_{step}^T \rightarrow \text{Sharer}$  // Record the mean interacting time from Step 1 to 5, and send it to the Sharer.  
  7. **if**  $\xi > 0$ :  $\text{sleep}(\xi)$  // Fetch the relative time  $\xi$  from the Sharer, and sleep for  $\xi$  seconds if the Actor runs faster.  
  8.  $\mathbf{s} = \mathbf{s}', T_{step} += N, \text{Sharer.buffer.size} += N$   
**end**

---

#### Algorithm 2: Learner

---

Initialize the Learner model parameters  $\theta_l$ , learning start steps  $C$ , model upload frequency  $U$ , and total backpropagation steps  $B_{step} = 0$ .  
**while**  $T_{step} < T$  **do**  
  **if**  $\text{Sharer.buffer.size} > C$  **then**  
    1.  $\mathbf{s}, \hat{\mathbf{a}}, \mathbf{r}, \mathbf{s}', \text{done} = \text{Sharer.buffer.sample}()$  // Sample a mini-batch of transitions from the Sharer.  
    2.  $\theta_l = \text{DRL}(\mathbf{s}, \hat{\mathbf{a}}, \mathbf{r}, \mathbf{s}', \text{done}; \theta_l)$  // Optimize the model with the underlying DRL algorithm.  
    3. **if**  $B_{step} \% U = 0$ :  $\theta_l \rightarrow \theta_s$  // Upload the latest model  $\theta_l$  to the Sharer at a fixed frequency  $U$ .  
    4.  $B_{step}^T \rightarrow \text{Sharer}$  // Record the mean optimization time from Step 1 to 3, and send it to the Sharer.  
    5. **if**  $\xi \leq 0$ :  $\text{sleep}(-\xi/\rho)$  // Fetch the relative time  $\xi$  from the Sharer, and sleep for  $-\xi/\rho$  seconds if the Learner runs faster.  
    6.  $B_{step} += 1$   
  **end**  
**end**

---

takes extensive exploration to pass the current scenario, only to find the exploration noise is decreased to a low level, and sufficient exploration can no longer be guaranteed in the new scenario. Contrastingly, the VEM divides the vectorized environments into **exploiting** interval (OI) and **exploring** interval (OR). As shown in Fig. 2, the exploration noises maintain the minimal value  $E_{min}$  in exploiting interval and are linearly interpolated from  $E_{min}$  to the maximal value  $E_{max}$  in the exploring interval. In addition, the exploring interval is linearly diminished to a certain extent during the training process. Relative to standard  $\epsilon$ -greedy exploration, the VEM inherits its positive attribute: progressively focus on exploitation during training. Meanwhile, the VEM also bypasses its flaw: conserve a sound exploration capability even in the final training stage. Consequently, the VEM reaches a more sensible balance between exploration and exploitation, thus enhancing the sample efficiency accordingly.

#### 3.1.2. Time feedback mechanism

In off-policy DRL with experience replay mechanism, one can train the model multiple times after one interaction with the environment or a single update after multiple interactions. To quantify the data utilization rate, we define the *Transitions Per Step (TPS)*:

$$TPS = \frac{B \times B_{step}}{T_{step}} \quad (1)$$

where  $B$  is the batch size,  $B_{step}$  is the total backpropagation steps (the number of times that the model has been optimized), and  $T_{step}$  is the total interacting steps. The *TPS* indicates how many transitions have been replayed for training per interaction. A large *TPS* implies a high data utilization rate but may also lead to model collapse due to data overuse [34]. Conversely, a small *TPS* results in data underuse, resulting in low sample efficiency. Since the Ape-X expedites the training at the expense of completely decoupling the interaction and optimization procedures without controlling the *TPS*, it is inevitable to incur a



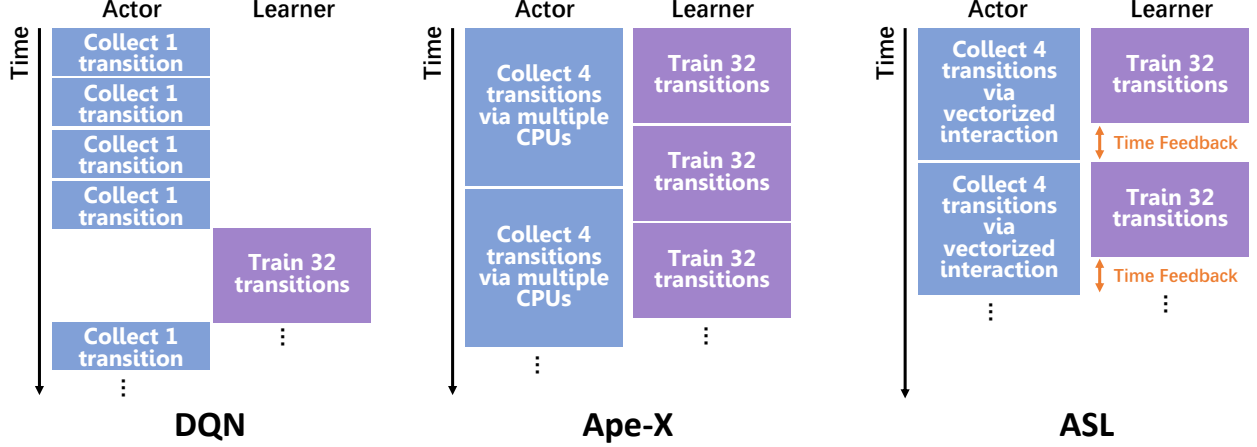


**Fig. 4.** Illustration of the coupled framework (left, representative: DQN), completely decoupled framework (middle, representative: Ape-X), and partially decoupled framework with TFM (right, representative: ASL). In this example, both the DQN and the ASL seek to maintain a  $TPS$  of 8. However, the cycle (the collection of 4 transitions + the training of 32 transitions) in DQN is more time-consuming due to its step-by-step collection and the alternation between collection and training. Conversely, the ASL demonstrates computational efficiency attributable to its vectorized interaction and its ability to perform collection and training concurrently. In contrast, the Ape-X fully decouples the collection and training processes, resulting in an uncontrolled  $TPS$  and risking its training stability and sample efficiency.

loss of stability or sample efficiency. In contrast, the ASL employs the TFM to modulate the relative speed between actor and learner, imposing a certain amount of dormant period upon the faster one of actor and learner to coordinate the  $TPS$  of the learning system, as illustrated by Fig. 4. In doing so, the data overuse or underuse phenomenon could be circumvented. In vectorized environments, based on (1), we have the following equation:

$$B_{step} = \frac{N \times TPS}{B} V_{step} \quad (2)$$

where  $N$  is the number of copies of vectorized environments and  $V_{step} = T_{step}/N$  is the total number of vectorized steps. To connect (2) with time feedback, we define the period, namely the elapsed time, of one VDC procedure and one model optimization procedure as  $V_{step}^T$  and  $B_{step}^T$ , respectively. We also use  $\rho$  to denote  $(N \times TPS)/B$  for brevity. Then, we have

$$\frac{\tau}{B_{step}^T} = \rho \frac{\tau}{V_{step}^T} \quad (3)$$

where  $\tau$  is the elapsed time of ASL. Evidently, the following equation holds:

$$V_{step}^T = \rho B_{step}^T \quad (4)$$

Eq. (4) suggests that by modulating the two elapsed times in a manner consistent with such relative relationship, a fixed  $TPS$  can be approximately upheld. To achieve this end, the actor and learner would record their individual period  $V_{step}^T$  and  $B_{step}^T$ . The sharer then coordinates their running speed according to the two following principles:

- if  $\xi = \rho B_{step}^T - V_{step}^T > 0$ , the actor sleeps for a period of  $\xi$  every after one VDC procedure.
- if  $\xi \leq 0$ , the learner sleeps for a period of  $-\xi/\rho$  every after one model optimization procedure.

Regarding the dormancy in TFM, one might wonder whether the TFM maintains the sample efficiency at the cost of sacrificing the training time efficiency, which deviates from our rudimentary purpose. Indeed, the dormancy could slow down the training framework to some extent but bring about a more sensible data recency, which tremendously facilitates model optimization. That is, reaching the same performance with fewer times of optimization, which conversely reduces the time needed for training.

### 3.1.3. Workflow of ASL

The pseudocode of ASL is given in Algorithm 1 and 2, and the corresponding schematic is shown in Fig 3. In ASL, the actor and learner run simultaneously until reaching the maximum interaction steps  $T$ . Note that, to avoid overfitting, the learner starts to learn only after a certain number of transitions have been collected.

### 3.2. Sparrow simulator

Sparrow is a mobile robot-oriented simulation platform, as shown in Fig. 5(a). The development of Sparrow is triggered by the niche, as detailed in Section 2, between two types of widely adopted simulators, the Gazebo and the Procgen. The Gazebo is inordinately heavy and thus forms an impediment to parallelization as well as diversity, while the Procgen is purely video game-oriented, unable to foster the real-world application of DRL. Consequently, we posed a question to ourselves: is it possible to propose a mobile robot-oriented simulator that is lightweight to expedite data acquisition and diversifiable to augment the generalization capacity of the trained agent?

To this end, we employed a 2D grid-based world and a simplified kinematic model to describe the obstacles and robot, circumventing the complicated physics calculation. As a result, the Sparrow occupies merely 30KB of hard disk and 140MB of the GPU memory. Even with extensive vectorization, the hardware resources would not be extravagantly consumed, which

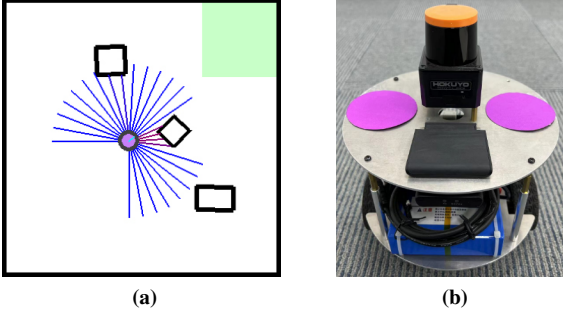


**Fig. 5.** (a) Sparrow simulator: the green area represents the target area; the black rectangles are the obstacles; the blue rays and purple circle denote the LiDAR and the robot, respectively. (b) Real-world counterpart of the robot in Sparrow: a differential wheeled robot.

prominently hastens the data collection by aggregating samples from more environmental copies under the same computational resources. More importantly, another noteworthy benefit brought about by lightness is vectorized diversity. That is, diversified simulation setups could be adopted by different copies of the vectorized environments and be simulated simultaneously. In doing so, diverse experiences could be generated by the Sparrow, and the generalization capability of the DRL agent is promising to be bolstered. Due to the limited scope, an exhaustive elucidation of Sparrow cannot be carried out in this paper but could be accessed on our website<sup>1</sup>. However, two key insights are essential for a more comprehensive understanding.

### 3.2.1. Simplified kinematic model

The kinematics of the robot in Sparrow is described as:

$$[V_l^{t+1}, V_a^{t+1}] = K \cdot [V_l^t, V_a^t] + (1 - K) \cdot [V_l^{target}, V_a^{target}] \quad (5)$$

where  $V$  denotes the velocity of the robot, the subscripts  $l$  and  $a$  are the respective abbreviations of linear and angular velocities, the superscripts  $t$  and  $target$  respectively represent the timestep and target velocity, and  $K$  is a hyperparameter between (0,1) that describes the combined effect of inertia, friction, and the underlying motion control algorithm. We simplify the kinematic model in this way for two reasons. First, such representation evades complicated physics calculation, conducing to the lightness of Sparrow. Second, we argue that it is inefficient or even unwise to separately investigate the coupling effects resulting from inertia, friction, and the underlying motion control algorithm due to their intricate interplay in the real world. Since these factors jointly affect how the velocity of the robot changes given the target velocity, we employed the parameter  $K$  to represent the final effects. Although  $K$  cannot be measured accurately in real-world or even varies in different scenarios, we can guarantee the effectiveness of the simplified kinematics by utilizing vectorized diversity to train a generalized agent.

### 3.2.2. Conversion-free data flow

Due to disparate implementation, most simulators to date have different data flow compared with the DRL algorithm.

Consequently, it is inevitable to perform certain data format conversions during training. A common case is from the *List* format in *Python*<sup>2</sup> (generated by the simulator, stored in RAM) to the *Tensor* format in *Pytorch*<sup>3</sup> (utilized by the deep neural networks, stored in GPU). Such conversion is tedious and time-consuming, which slows down the training and can be even aggravated in a large-scale learning framework that requires high data throughput. To tackle this issue, we implemented the Sparrow with the prevalent machine learning framework *Pytorch* such that the data generated by Sparrow is already in *Pytorch.Tensor* format, thus obviating the conversion procedure.

### 3.3. Color

Having comprehended the ASL framework and the Sparrow simulator, the only remaining question pertains to their optimal amalgamation. That is, forming a comprehensive solution that enables the efficient training of a DRL agent with adequate resilience to generalize over a series of analogous scenarios as well as the real-world scenario. Our method, named Color, is illustrated in Fig. 1, wherein the ASL and the Sparrow are seamlessly integrated by their interdependent vectorized environments, and the training maps and simulation parameters are randomized in different copies of the vectorized environments of Sparrow. Through interacting with the vectorized and diverse environments, the actor of ASL is empowered to gather a collection of “colorful” experiences, which is then preserved in the sharer and prepared for the model optimization of the learner. In this fashion, the efficiency of our method is guaranteed by the ASL framework, and the generalization of the trained agent is promised by learning from the “colorful” experience generated by Sparrow.

## 4. Experiments

In this section, we conduct four distinct types of experiments to substantiate the superiority of the proposed methods. The first experiment focuses on the efficiency of the ASL framework. Comprehensive experiments have been conducted on 57 Atari games [35], and the results are compared with other previously published DRL baselines. The second experiment involves a comparative study of Sparrow and other prevalent simulators. The final two experiments examine the Task2Task and Sim2Real capabilities of the agent derived from Color.

### 4.1. Evaluation of ASL

#### 4.1.1. Experiment setup on Atari

The Atari environment, composed of 57 video games, is a standardized platform commonly employed by the DRL communities. The high-dimensional visual input and the sparse rewards of Atari form a collection of challenging tasks, making it a valuable tool for the evaluation and comparison of different algorithms. To validate the efficiency of ASL, its results on 57

<sup>1</sup><https://github.com/XinJingHao/Color>

<sup>2</sup><https://www.python.org>

<sup>3</sup><https://pytorch.org>

Table 1: Raw Score Comparison Across 57 Atari Games

Game	Random	DQN	DDQN	Prior. DDQN	Duel. DDQN	Noisy DQN	DSQN	Ape-X DDQN	ASL DDQN (Ours)	Ipv1	Ipv2
Alien	227.8	3,069.0	2,907.3	4,203.8	4,461.4	2,403.0	-	2,596.1	<b>6,955.2</b>	251.1%	284.1%
Amidar	5.8	739.5	702.1	1,838.9	<b>2,354.5</b>	1,610.0	-	1,271.2	2,232.3	319.8%	176.0%
Assault	222.4	3,359.0	5,022.9	7,672.1	4,621.0	5,510.0	-	<b>14,490.1</b>	14,372.8	294.8%	99.2%
Asterix	210.0	6,012.0	15,150.0	31,527.0	28,188.0	14,328.0	-	189,300.0	<b>567,640.0</b>	3798.1%	300.1%
Asteroids	719.1	1,629.0	930.6	2,654.3	2,837.7	<b>3,455.0</b>	-	1,107.9	1,984.5	598.3%	325.5%
Atlantis	12,850.0	85,641.0	64,758.0	357,324.0	382,572.0	923,733.0	487,366.7	831,952.0	<b>947,275.0</b>	1800.2%	114.1%
BankHeist	14.2	429.7	728.3	1,054.6	<b>1,611.9</b>	1,068.0	-	1,264.9	1,340.9	185.8%	106.1%
BattleZone	2,360.0	26,300.0	25,730.0	31,530.0	37,150.0	36,786.0	-	38,671.0	<b>38,986.0</b>	156.7%	100.9%
BeamRider	363.9	6,846.0	7,654.0	23,384.2	12,164.0	20,793.0	7,226.9	<b>27,033.7</b>	26,841.6	363.2%	99.3%
Berzerk	123.7	-	-	1,305.6	1,472.6	905.0	-	924.8	<b>2,597.2</b>	-	308.8%
Bowling	23.1	42.4	70.5	47.9	65.5	<b>71.0</b>	-	60.2	62.4	82.9%	105.9%
Boxing	0.1	71.8	81.7	95.6	99.4	89.0	95.3	99.4	<b>99.6</b>	121.9%	100.2%
Breakout	1.7	401.2	375.0	373.9	345.3	516.0	386.5	370.7	<b>621.7</b>	166.1%	168.0%
Centipede	2,090.9	<b>8,309.0</b>	4,139.4	4,463.2	7,561.4	4,269.0	-	3,808.4	3,899.8	88.3%	105.3%
ChopperCommand	811.0	6,687.0	4,653.0	8,600.0	11,215.0	8,893.0	-	6,031.0	<b>15,071.0</b>	371.2%	273.2%
CrazyClimber	10,780.5	14,103.0	101,874.0	141,161.0	143,570.0	118,305.0	123,916.7	118,020.0	<b>166,019.0</b>	170.4%	144.8%
Defender	2,874.5	-	-	31,286.5	<b>42,214.0</b>	20,525.0	-	29,255.0	37,026.5	-	129.5%
DemonAttack	152.1	9,711.0	9,711.9	71,846.4	60,813.3	36,150.0	-	114,874.7	<b>119,773.9</b>	1251.3%	104.3%
DoubleDunk	-18.6	-18.1	-6.3	<b>18.5</b>	0.1	1.0	-	-0.2	0.1	152.0%	101.6%
Enduro	0.0	301.8	319.5	2,093.0	<b>2,258.2</b>	1,240.0	-	1,969.1	2,103.1	658.2%	106.8%
FishingDerby	-91.7	-0.8	20.3	39.5	<b>46.4</b>	11.0	-	31.2	35.1	113.2%	103.2%
Freeway	0.0	30.3	31.8	33.7	0.0	32.0	-	21.4	<b>33.9</b>	106.6%	158.4%
Frostbite	65.2	328.3	241.5	4,380.1	4,672.8	753.0	-	504.7	<b>8,616.4</b>	4850.4%	1945.7%
Gopher	257.6	8,520.0	8,215.4	32,487.2	15,718.4	14,574.0	10,107.3	47,845.6	<b>103,514.4</b>	1297.6%	217.0%
Gravitar	173.0	306.7	-	548.5	588.0	447.0	-	242.5	<b>760.0</b>	-	844.6%
Hero	1,027.0	19,950.0	20,357.0	23,037.7	20,818.2	6,246.0	-	14,464.0	<b>26,578.5</b>	132.2%	190.2%
IceHockey	-11.2	-1.6	-2.4	<b>1.3</b>	0.5	-3.0	-	-2.5	-3.6	86.4%	87.4%
Jamesbond	29.0	576.7	438.0	<b>5,148.0</b>	1,312.5	1,235.0	1,156.7	540.0	2,237.0	539.9%	432.1%
Kangaroo	52.0	6,740.0	13,651.0	<b>16,200.0</b>	14,854.0	10,944.0	8,880.0	14,710.0	13,027.0	95.4%	88.5%
Krull	1,598.0	3,805.0	4,396.7	9,728.0	<b>11,451.9</b>	8,805.0	9,940.0	10,999.4	10,422.5	315.3%	93.9%
KungFuMaster	258.5	23,270.0	29,486.0	39,581.0	34,294.0	36,310.0	-	54,124.0	<b>85,182.0</b>	290.6%	157.7%
MontezumaRevenge	0.0	0.0	0.0	0.0	0.0	<b>3.0</b>	-	0.0	0.0	-	-
MsPacman	307.3	2,311.0	3,210.0	<b>6,518.7</b>	6,283.5	2,722.0	-	4,087.7	4,416.0	141.5%	108.7%
NameThisGame	2,292.3	7,257.0	6,997.1	12,270.5	11,971.1	8,181.0	10,877.0	16,042.7	<b>16,535.4</b>	302.7%	103.6%
Phoenix	761.4	-	-	18,992.7	23,092.2	16,028.0	-	28,296.0	<b>71,752.6</b>	-	257.8%
Pitfall	-229.4	-	-	-356.5	<b>0.0</b>	<b>0.0</b>	-	<b>0.0</b>	<b>0.0</b>	-	100.0%
Pong	-20.7	18.9	<b>21.0</b>	20.6	<b>21.0</b>	<b>21.0</b>	20.3	<b>21.0</b>	<b>21.0</b>	100.0%	100.0%
PrivateEye	24.9	1,788.0	670.1	200.0	103.0	<b>3,712.0</b>	-	173.0	349.7	50.3%	219.3%
Qbert	163.9	10,596.0	14,875.0	16,256.5	19,220.3	15,545.0	-	15,300.0	<b>24,548.8</b>	165.8%	161.1%
Riverraid	1,338.5	8,316.0	12,015.3	14,522.3	21,162.6	9,425.0	-	22,238.0	<b>24,445.0</b>	216.4%	110.6%
RoadRunner	11.5	18,257.0	48,377.0	57,608.0	<b>69,524.0</b>	45,993.0	48,983.3	51,208.0	56,520.0	116.8%	110.4%
Robotank	2.2	51.6	46.7	62.6	65.3	51.0	-	42.6	<b>65.8</b>	142.9%	157.4%
Seaquest	68.4	5,286.0	7,995.0	26,357.8	<b>50,254.2</b>	2,282.0	-	32,101.8	29,278.6	368.5%	91.2%
Skiing	-17,098.1	-	-	-9,996.9	-8,574.4	-14,763.0	-	-15,623.8	<b>-8,295.4</b>	-	597.1%
Solaris	1,236.3	-	-	4,309.0	2,250.8	<b>6,088.0</b>	-	1,523.2	3,506.8	-	791.4%
SpaceInvaders	148.0	1,976.0	3,154.6	2,865.8	6,427.3	2,186.0	1,832.2	3,943.0	<b>21,602.0</b>	713.6%	565.3%
StarGunner	664.0	57,997.0	65,188.0	63,302.0	89,238.0	47,133.0	57,686.7	60,835.0	<b>129,140.0</b>	199.1%	213.5%
Surround	-10.0	-	-	<b>8.9</b>	4.4	-1.0	-	2.9	2.5	-	96.9%
Tennis	-23.8	-2.5	1.7	0.0	5.1	0.0	-1.0	-0.9	<b>22.3</b>	180.8%	201.3%
TimePilot	3,568.0	5,947.0	7,964.0	9,197.0	11,666.0	7,035.0	-	7,457.0	<b>12,071.0</b>	193.4%	218.6%
Tutankham	11.4	186.7	190.6	204.6	211.4	232.0	194.7	226.2	<b>252.9</b>	134.8%	112.4%
UpNDown	533.4	8,456.0	16,769.9	16,154.1	44,939.6	14,255.0	-	<b>46,208.0</b>	25,127.4	151.5%	53.8%
Venture	0.0	380.0	93.0	54.0	<b>497.0</b>	97.0	-	62.0	291.0	312.9%	469.4%
VideoPinball	16,256.9	42,684.0	70,009.0	282,007.3	98,209.5	322,507.0	275,342.8	603,075.0	<b>626,794.0</b>	1135.8%	104.0%
WizardOfWor	563.5	3,393.0	5,204.0	4,802.0	7,855.0	9,198.0	-	14,780.0	<b>21,049.0</b>	441.5%	144.1%
YarsRevenge	3,092.9	-	-	11,357.0	<b>49,622.1</b>	23,915.0	-	13,178.5	29,231.9	-	259.2%
Zaxxon	32.5	4,977.0	10,182.0	10,469.0	12,944.0	6,920.0	-	-	<b>16,420.0</b>	161.5%	-

Scores of Random, Prior. DDQN, and Duel. DDQN are taken from [9].

Scores of DQN, Noisy DQN, DDQN, and DSQN are taken from [5, 36, 10, 37], respectively.

Since Ape-X did not publish its score combining with DDQN, the scores of Ape-X DDQN and ASL DDQN are both obtained by our experiments.

**Ipv1** = (ASL DDQN - Random)/(DDQN - Random): the improvement of ASL DDQN over its underlying DRL algorithm DDQN.

**Ipv2** = (ASL DDQN - Random)/(Ape-X DDQN - Random): the improvement of ASL DDQN over Ape-X DDQN.

Atari games are compared with DQN [5], DDQN [36], Prior. DDQN [11], Duel. DDQN [9], Noisy DQN [10] and DSQN [37]. Essentially, ASL is a DRL training framework and should be applied in conjunction with a specific DRL algorithm. Although extensive improvement techniques have emerged since the ground-breaking work of DQN, we choose to combine the ASL framework merely with the DDQN, an algorithm that mitigates the notorious overestimation problem of DQN by Double Q-learning, and omit other tricks such as PER, dueling network, noisy network, etc. We do this with the intention of prevent-

ing these techniques from submerging the ASL. In this context, we refer to our algorithm as ASL DDQN. In addition, since the ASL is mostly inspired by the Ape-X framework, we also compare our algorithm with the Ape-X DDQN. For a fair comparison, we follow the experimental setup of previous works. We employ the same Atari preprocess procedures and model architecture of DDQN. Furthermore, we also adopt the no-ops scheme, which imposes a random number (upper-bounded by 30) of no-op actions at the beginning of each episode. The no-ops scheme could effectively prevent the agent from overfitting

when training while also examine its robustness when evaluating. In addition, the episode of each Atari game is terminated at 12.5K steps and 27K steps for training and evaluation, respectively.

Regarding the hyperparameters, since the ASL DDQN is constituted of a training framework and a DRL algorithm, the hyperparameters consist of two parts as well. Considering the prohibitively high cost of fulfilling an exhaustive search on the combined hyperparameter space, we determine the algorithm-associated hyperparameters based on the published papers and the framework-relevant hyperparameters mostly by manual coordinate descent. For instance, we did not observe a noticeable impact of the model upload frequency  $U$  and therefore made an accommodation between the model recency and transmission cost. In addition, the number of vectorized environments  $N$  is assigned a value of 128 to correspond with the maximum capacity of our CPU (AMD 3990X, 64 cores, 128 threads). The  $TPS$  is set to 8, the same as DDQN (a backpropagation with a mini-batch of size 32 every after 4 transitions have been collected). More information about the hyperparameter is listed in Table 3. Note that the hyperparameters across all 57 Atari games are identical.

The ASL DDQN and Ape-X DDQN are trained for 50M and 500M  $T_{step}$ , respectively. During the training, the model is evaluated every 5K  $B_{step}$ . Fig. 11 and Fig. 12 from the Appendix compare the ASL DDQN and Ape-X DDQN in terms of sample efficiency and training time efficiency, respectively. After training, the best models of the 57 Atari games are evaluated for 100 episodes, and the averaged raw scores are compared with other DRL baselines published previously, as the results presented in Table 1.

#### 4.1.2. Sample efficiency

It can be observed from Fig. 11 that the ASL framework substantially improved the sample efficiency over the Ape-X framework, reaching the equivalent or remarkably better performance with considerably less training data. We contend that the improvement originates from the TFM and the VEM. The relative speed of the Actor and Learner is reasonably coordinated by the TFM in accordance with the  $TPS$ , preventing the Actor from generating redundant data. Meanwhile, the VEM overcomes the limitation of canonical  $\epsilon$ -greedy exploration, reaching a more rational compromise between exploration and exploitation and yielding higher quality training data.

#### 4.1.3. Training time efficiency

Fig. 12 suggests that ASL outperforms Ape-X in terms of training time efficiency, capable of achieving superior performance under an identical period of time on most of the Atari games. We posit that the superiority of ASL is attributed to the VDC mode and the TFM. As detailed previously, the VDC mode harnesses the parallel processing capabilities of GPU to the fullest extent and simplifies the data preservation, which elevates the computational efficiency and shortens the training time consequently. Furthermore, the prudent data recency upheld by the TFM significantly fosters the model optimization,

resulting in comparable performance with fewer training instances and thus decreasing overall required training time.

#### 4.1.4. Stability

The ASL framework exhibits better stability than Ape-X, which is supported by the curves from *Freeway*, *Frostbite*, and *Zaxxon*, where the Ape-X DDQN failed to learn. We conjecture such failures are mostly incurred by the uncontrolled  $TPS$  in Ape-X.

#### 4.1.5. Final performance

Table 1 reveals that the ASL DDQN outstrips other DRL baselines over 32 Atari games. Besides, the final performance gain achieved by the ASL DDQN over its underlying algorithm DDQN is a remarkable 508.2% (averaged over *Ipv1* across 57 Atari games). Furthermore, compared to the framework counterpart Ape-X, the ASL demonstrates a substantial improvement of 234.9% (averaged over *Ipv2* across 57 Atari games). These findings provide strong evidence of the superiority of our ASL training framework.

#### 4.2. Simulator comparison

To demonstrate the superiority of Sparrow, it is compared with four widely adopted DRL simulators. For a fair comparison, analogous layouts are constructed within the mobile robot-oriented simulators, as shown in Fig. 6. The comparison results are presented in Table 2.

As delineated in Table 2, Sparrow encompasses a series of advantageous features, namely RL-API, Vectorization, and DR. These attributes, often overlooked by alternative mobile robot simulators, are instrumental for DRL training, as they facilitate deployment, boost the training speed, and enhance the generalization ability of the trained agent. Concurrently, Sparrow provides a conversion-free data flow, thereby eliminating the need for data conversion between GPU and RAM, a common bottleneck in training speed. Moreover, Sparrow is the most resource-efficient among the five simulators under consideration in terms of both GPU memory and hard disk usage. To quantify the simulation speed, we employ the maximal RTF, defined as the ratio of the simulated time to the real time when running the simulator at peak speed. Although Sparrow is not the fastest in the single environment setting ( $N=1$ ), its simulation speed could be substantially promoted through vectorization. With a vectorization of 64 copies, Sparrow achieves a maximal RTF of 815.5, remarkably surpassing the other two mobile robot-oriented simulators. In summary, we posit that Sparrow has bridged the niche between two types of simulators: a) physical simulators such as Gazebo and Webots, which lack vectorization to boost data throughput and DR to enhance the generalization capability of the trained DRL agent, and b) game simulators like CoinRun and Procgen, which are limited in their contribution to real-world applications of DRL.

Finally, we would like to introduce three promising applications of Sparrow. First, as well as the most discussed, Sparrow is capable of fostering the efficiency and generalization of the trained DRL algorithm by providing vectorized diversity. Second, the broad trend in the DRL community to date is evaluating



Table 2: Simulator Comparison

Simulator	Vectorization	DR	RL-API	CFDF	Robot-oriented	Maximal RTF	GPU Memory (MB)	Hard Disk (MB)
Sparrow (Ours)	✓	✓	✓	✓	✓	$N1$ : 24.3 $N64$ : <b>815.5</b>	$N1$ : <b>140</b> $N64$ : <b>140</b>	<b>0.03</b>
Gazebo [27]	✗	✗	✗	✗	✓	16.2	180	170
Webots [38]	✗	✗	✗	✗	✓	113.9	560	456
CoinRun [26]	✓	✓	✓	✗	✗	-	-	38.8
Progen [21]	✓	✓	✓	✗	✗	-	-	36.6

DR: Domain randomization [16]; RL-API: Reinforcement learning application programming interfaces such as *reset()* and *step()*; CFDF: Conversion-free data flow; RTF: Real-time factor;  $N$ : Number of vectorized environments.

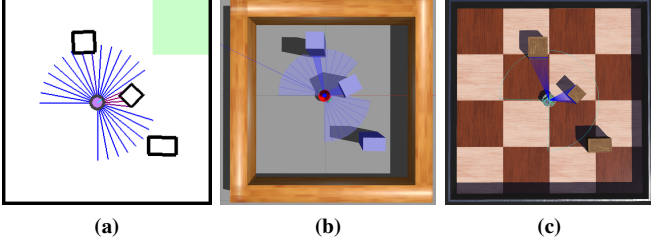


Fig. 6. Comparison between different mobile robot-oriented simulators: (a) Sparrow, (b) Gazebo, (c) Webots.

the performance of agent on the training environment. We contend such evaluation is irrational to some extent because it is equivalent to evaluate on the training set in supervised learning. Thanks to the diversifiable characteristics of Sparrow, it is feasible to quantify the generalization of the DRL agent more precisely by constructing different simulation parameters or maps during evaluation. Last, the lightness and the conversion-free data flow of Sparrow render it notably user-friendly, thereby promoting the potential for expeditious deployment, assessment, and comparison of DRL algorithms. For these reasons, we hold the belief that Sparrow could be deemed as a holistic simulation platform and would profitably contribute to the community of DRL researchers and practitioners.

#### 4.3. Task2Task generalization

##### 4.3.1. Problem formulation

The experiments of this section are conducted on the Sparrow simulator, wherein the LPP problem is formulated as a Markov Decision Process (MDP) to enable the employment of DRL. At timestep  $t$ , the agent observes the state  $s_t$  from the environment, takes the action  $a_t$  according to its policy  $\pi$ , receives the reward  $r_t$ , and subsequently transits to the next state  $s_{t+1}$ , with the objective of maximizing the expected sum of discounted rewards  $\mathbb{E}_\pi \left[ \sum_{t=0}^{+\infty} \gamma^t r_t \right]$ , where  $\gamma \in [0, 1]$  is the discount factor.

**State:** The state of the agent is a vector of length 32, containing the pose of the robot ( $dx$ ,  $dy$  and  $\alpha$  as shown in Fig. 7(a)), the linear and angular velocity of the robot ( $V_l$  and  $V_a$ ), and 27 scanning results of the LiDAR mounted on the robot. The state variables will be normalized and represented in a relative fashion before being fed to the agent. The normalized relative state representation could simplify the training: we could train the agent in a fixed manner (start from the lower left corner, and end at the upper right corner), and the trained agent is capable

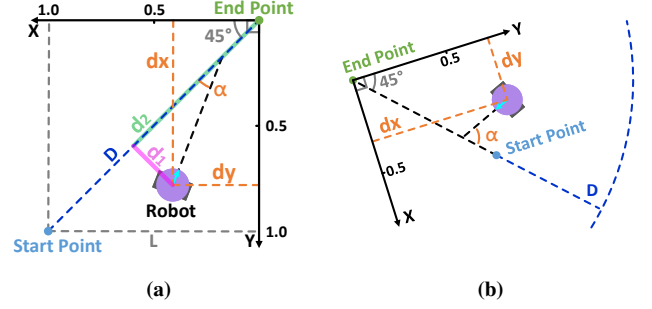


Fig. 7. Normalized relative state representation of Sparrow. Here,  $L$  is the training map size, and  $D$  is the maximum local planning distance.

of handling any start-end scenarios as long as their distance is within  $D$ , as illustrated in Fig. 7(b).

**Action:** We employ 5 discrete actions to control the target velocity  $[V_l^{target}, V_a^{target}]$  of the robot, which are:

- *Turn left*: [0.36 cm/s, 1 rad/s]
- *Go straight and turn left*: [18 cm/s, 1 rad/s]
- *Go straight*: [18 cm/s, 0 rad/s]
- *Go straight and turn right*: [18 cm/s, -1 rad/s]
- *Turn right*: [0.36 cm/s, -1 rad/s]

**Reward:** If the robot collides with an obstacle or reaches the end point, the episode is terminated, and the agent is rewarded with -10 or 75, respectively. Otherwise, the agent receives a reward according to:

$$r = 0.3r_{d1} + 0.1r_{d2} + 0.3r_v + 0.3r_\alpha + 0.1r_d \quad (6)$$

where  $r_{d1}$  and  $r_{d2}$  are negatively correlated to  $d1$  and  $d2$  (refer to Fig. 7(a)), with a maximum value of 1;  $r_v = 1$  if the linear velocity of the robot exceeds half of its maximum linear velocity, otherwise 0;  $r_\alpha$  is negatively correlated to the absolute value of  $\alpha$ ;  $r_d = -1$  if the closest distance between the robot and an obstacle is smaller than 30 cm, otherwise 0. The reward function is devised with the intention of driving the robot to the end point expeditiously without colliding with obstacles. For more implementation details, please refer to our website<sup>1</sup>.

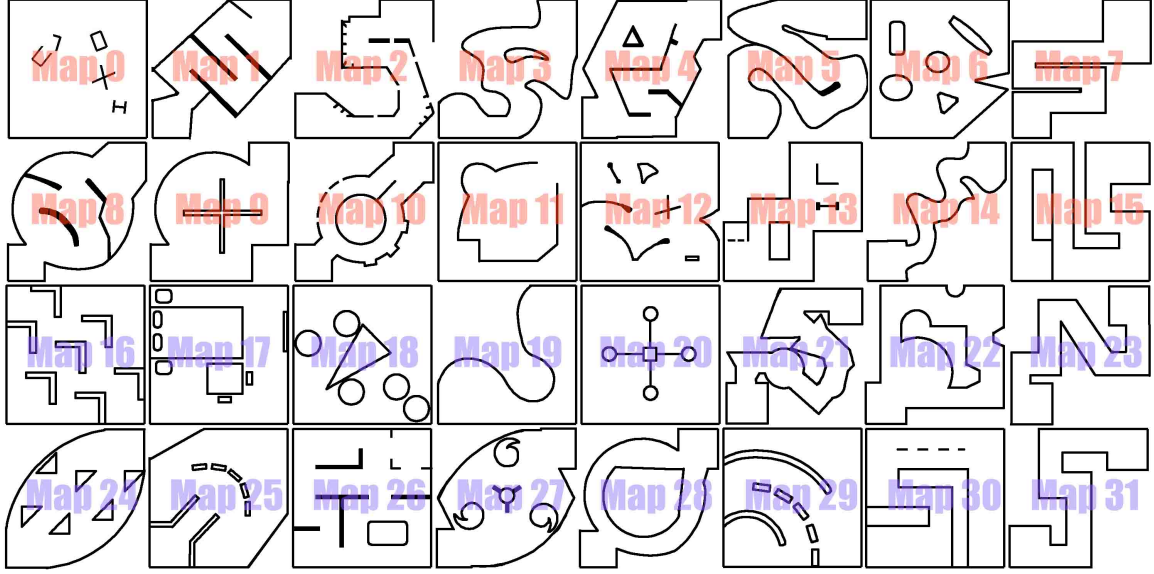


Fig. 8. Training (0~15) and test (16~31) maps for Task2Task generalization assessment.

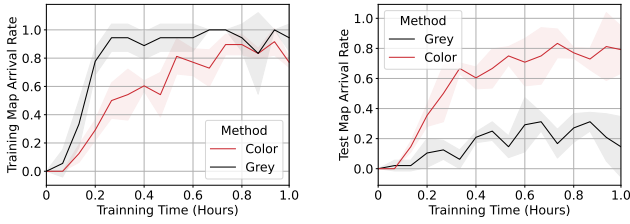


Fig. 9. Target area arrival rate on training maps (left) and test maps (right). The solid curves represent the mean value across three random seeds, and the translucent areas correspond to the standard deviation.

#### 4.3.2. Experiment setup on Sparrow

In this section, we seek to investigate the extent to which the vectorized diversity of Sparrow contributes to the Task2Task generalization of the trained agent. To achieve this goal, two experiment setups have been designed. The first setup, denoted as Grey, employs identical simulation parameters and training maps (Map0×16) across all vectorized environments. In contrast, the other setup, referred to as Color, randomizes the control interval, control delay, velocity range, kinematic parameter  $K$ , and the magnitude of sensor noise across the vectorized environments. Note that the initial values of these simulation parameters are roughly measured from our real-world robot as shown in Fig. 5(b). The randomization is realized by uniformly sampling from a moderate interval around the initial values, which is performed at the onset of each episode. Additionally, a collection of diverse maps is leveraged for training, as the Map0 to Map15 shown in Fig. 8. Notably, both Grey and Color employ the ASL training framework.

It is worth noting that, both for Grey and Color, the obstacles in Map0 and the initial pose of the robot are randomly generated to evade overfitting. We harness 4 fully connected layers of shape [32, 256, 128, 5] to map the state variable to the dis-

crete actions. Other hyperparameters are listed in Table 3. The Color and Grey were trained until converged under three different random seeds, approximately equating to one hour of wall-clock time per seed. During training, the models of Color and Grey were evaluated on their respective training maps and the common test maps (Map16 to Map31), and the corresponding target area arrival rate curves were recorded in Fig. 9.

#### 4.3.3. Analysis

Fig. 9 demonstrates that the overfitting, analogous to that in supervised learning, also occurs in DRL. As mirrored by the Grey, the homogeneous environments could result the DRL agent in overfitting and impair its generalization capability. Impressively, thanks to the diversified environment setups, the Color is able to achieve an arrival rate over 80% on the zero-shot generalization tests, with a tolerable loss of converge speed and final performance on training maps. These results validly corroborate the beneficial impact of Sparrow’s vectorized diversity on Task2Task generalization.

#### 4.4. Sim2Real generalization

As shown in Fig. 10, 36 real-world scenarios of 6 types have been built to examine the Sim2Real generalization capability of the agent trained by Color. We select the best performing model derived from previous section as the final planning model. To demonstrate the superiority of Color, the model is directly implanted into the robot (see Fig. 5(b)) to undertake the LPP task in the real world without any additional tuning or adaption. Impressively, the agent demonstrates superior proficiency in real-world local path planning, succeeding in navigating to the end point in 33 out of 36 total scenarios. The three failed cases have been designated in red within Fig. 10. It can be observed from the experiment video<sup>1</sup> that these failures are primarily induced by the robot’s attempts to forcefully navigate through obstacles. We believe that a more appropriate reward function or judicious

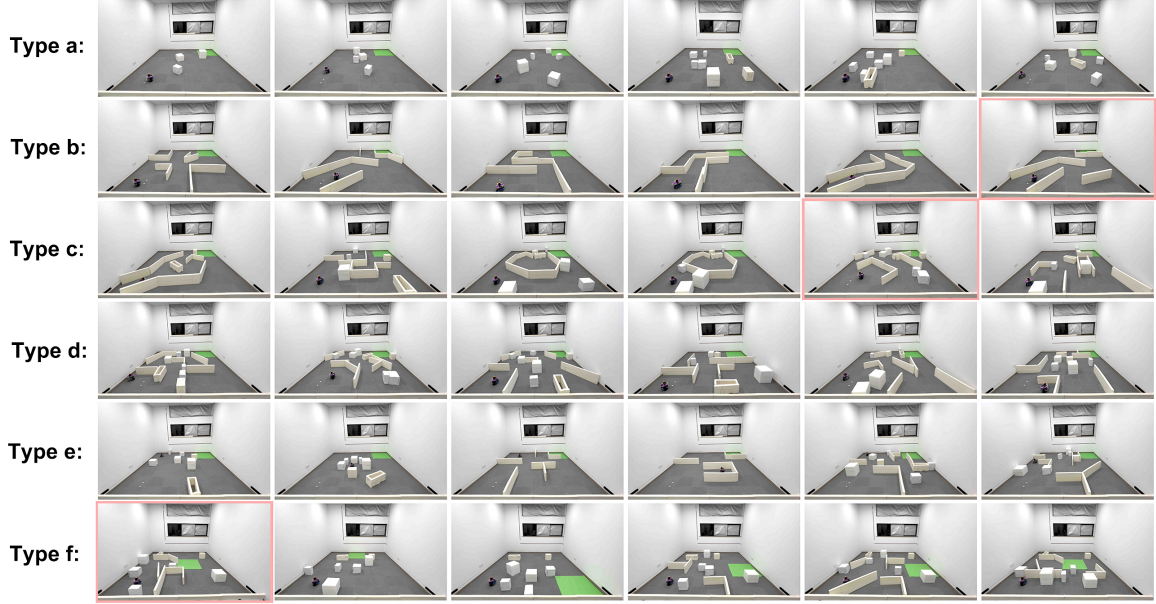


**Fig. 10.** 36 real-world scenarios for Sim2Real assessment: a) Blocky; b) Fence-shaped; c) Simply mixed; d) Intricately mixed; e) Random start point; f) Random end point. The task is to navigate the robot to the green area without collision. Failed cases are marked with red boxes. The video is available on the website<sup>1</sup>.

selection of the diverse training maps could further mitigate such issues, which will be the focus of our future works.

Compared with other solutions concerning the real-world application of DRL in the context of local planning or navigation, the advantages of Color can be more intuitively sensed. In [39], it takes approximately 30 hours of simulation training to derive a planner compatible with real-world environments. In [40], human guidance is indispensable to fine-tune the agent in the real world following simulation training. In [41], a mathematical model of the robot is required to model the discrepancy between the simulation and the real world. In contrast, our approach is entirely model-free. With merely one hour of simulation training, devoid of any human intervention, the agent is proficient in managing a variety of local planning tasks, both in simulation and the real world.

## 5. Conclusion

To improve the efficiency of the DRL algorithms, a partially decoupled training framework ASL is proposed. It is noteworthy that the ASL is specifically tailored to accommodate off-policy DRL algorithms that utilize experience replay. DRL algorithms that satisfy this requirement are well-suited for integration with ASL to enjoy a further promotion. In addition, a Sparrow simulator that supports vectorized diversity is developed to enhance the generalization capability of the ASL framework. The Sparrow and the ASL then are seamlessly integrated by their interdependent vectorized environments, resulting in a DRL solution to the LPP problem, namely Color. Impressively, with one hour of simulation training, the Color agent accomplished 33 out of 36 real-world LPP tasks, which we believe have reached a new milestone in the real-world application of DRL.

## Acknowledgement

We acknowledge the support from the National Natural Science Foundation of China under Grant No. 62273230 and 62203302.

We also acknowledge the support from the Ministry of Education, Singapore, under its Academic Research Fund Tier 1 (RG136/22). Any opinions, findings and conclusions or recommendations expressed in this material are those of the authors and do not reflect the views of the Ministry of Education, Singapore.

## Appendix

Table 3: Hyperparameters

Framework-associated	Atari	Sparrow
$N$	128	16
$TPS$	8	256
Linear Decay Steps of $OR$	500K $T_{step}$	500K $T_{step}$
$OR$	$128 \rightarrow 4$	$16 \rightarrow 3$
$E_{min}$	0.01	0.01
$E_{max}$	0.8	0.8
$U$	50 $B_{step}$	50 $B_{step}$
Algorithm-associated	Atari	Sparrow
Learning Start Steps $C$	150K transitions	30K transitions
Replay Buffer Size	1M transitions	1M transitions
$\gamma$	0.99	0.98
Learning rate	$6.25 \times 10^{-5}$	$1.0 \times 10^{-4}$
Target Net Update Frequency	2k $B_{step}$	200 $B_{step}$
Mini-batch size	32	256
Optimizer	Adam	Adam

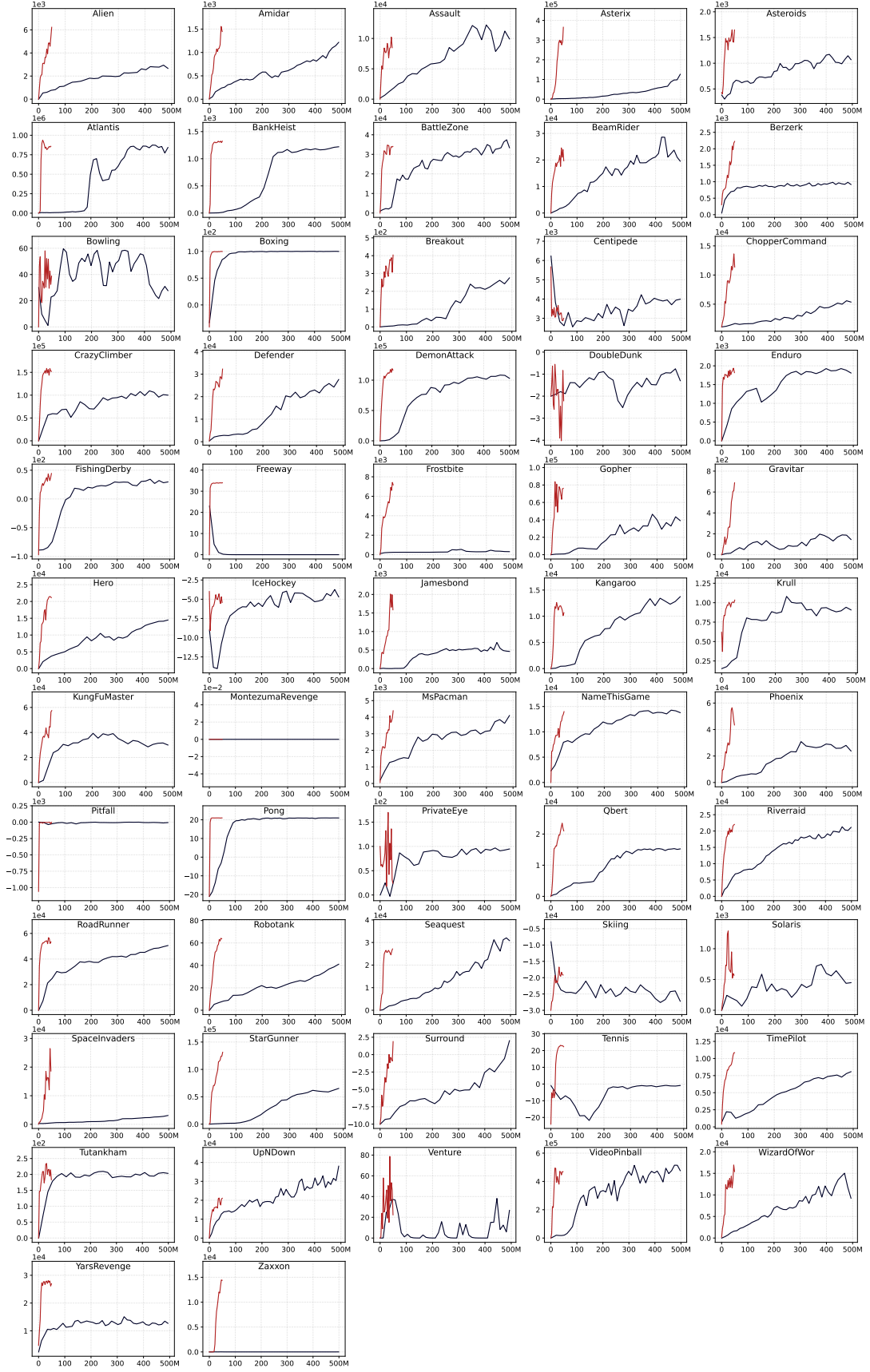


**Fig. 11.** Sample efficiency comparison between ASL DDQN (red) and Ape-X DDQN (dark). The horizontal axis is the number of transitions used during training, and the vertical axis is the episode reward of a single evaluation. The curves are exponentially smoothed by a factor of 0.95 to enhance readability.



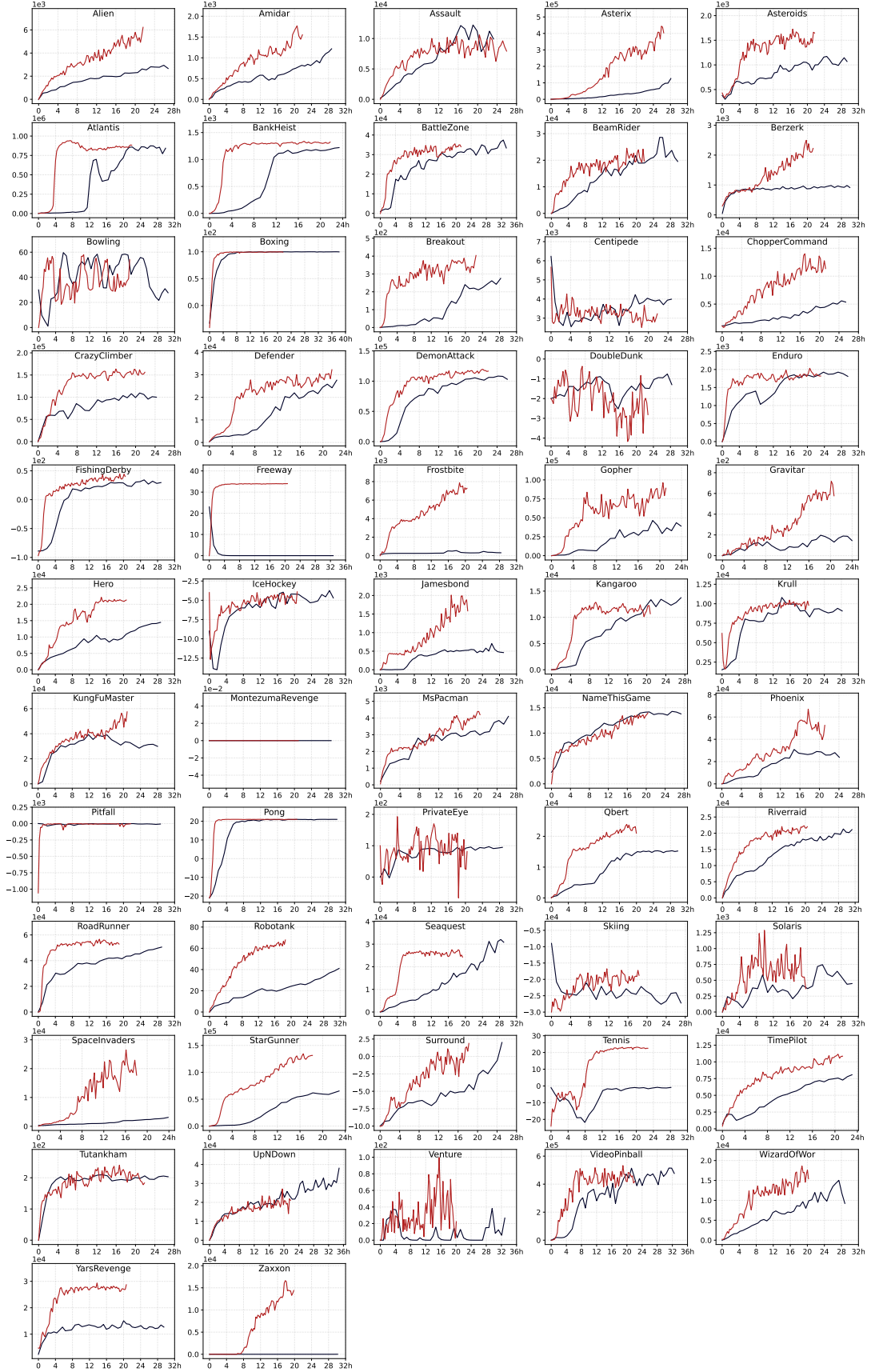


**Fig. 12.** Training time efficiency comparison between ASL DDQN (red) and Ape-X DDQN (dark). The horizontal axis is the training time, and the vertical axis corresponds to the episode reward of a single evaluation. The curves are exponentially smoothed by a factor of 0.95 to enhance readability.

## References

- [1] D. Fox, W. Burgard, S. Thrun, The dynamic window approach to collision avoidance, *IEEE Robotics & Automation Magazine* 4 (1) (1997) 23–33.
- [2] O. Cordón, F. Herrera, E. Herrera-Viedma, M. Lozano, Genetic algorithms and fuzzy logic in control processes, *Archives Of Control Science* 5 (1996) 135–168.
- [3] D. Kiss, G. Tevesz, Advanced dynamic window based navigation approach using model predictive control, in: 2012 17th International Conference on Methods & Models in Automation & Robotics (MMAR), IEEE, 2012, pp. 148–153.
- [4] C. Cheng, Q. Sha, B. He, G. Li, Path planning and obstacle avoidance for auv: A review, *Ocean Engineering* 235 (2021) 109355.
- [5] V. Mnih, K. Kavukcuoglu, D. Silver, A. A. Rusu, J. Veness, M. G. Bellemare, A. Graves, M. Riedmiller, A. K. Fidjeland, G. Ostrovski, et al., Human-level control through deep reinforcement learning, *nature* 518 (7540) (2015) 529–533.
- [6] D. Silver, A. Huang, C. J. Maddison, A. Guez, L. Sifre, G. Van Den Driessche, J. Schrittwieser, I. Antonoglou, V. Panneershelvam, M. Lanctot, et al., Mastering the game of go with deep neural networks and tree search, *nature* 529 (7587) (2016) 484–489.
- [7] S. Jin, X. Wang, Q. Meng, Spatial memory-augmented visual navigation based on hierarchical deep reinforcement learning in unknown environments, *Knowledge-Based Systems* (2023) 111358.
- [8] OpenAI, Gpt-4 technical report (2023). [arXiv:2303.08774](https://arxiv.org/abs/2303.08774).
- [9] Z. Wang, T. Schaul, M. Hessel, H. Hasselt, M. Lanctot, N. Freitas, Dueling network architectures for deep reinforcement learning, in: *Proceedings of The 33rd International Conference on Machine Learning*, Vol. 48, 2016, pp. 1995–2003.
- [10] M. Fortunato, M. G. Azar, B. Piot, J. Menick, M. Hessel, I. Osband, A. Graves, V. Mnih, R. Munos, D. Hassabis, O. Pietquin, C. Blundell, S. Legg, Noisy networks for exploration, in: *International Conference on Learning Representations*, 2018.
- [11] T. Schaul, J. Quan, I. Antonoglou, D. Silver, Prioritized experience replay, in: *International Conference on Learning Representations*, 2016.
- [12] Q. Wei, H. Ma, C. Chen, D. Dong, Deep reinforcement learning with quantum-inspired experience replay, *IEEE Transactions on Cybernetics* 52 (9) (2021) 9326–9338.
- [13] V. Mnih, A. P. Badia, M. Mirza, A. Graves, T. Lillicrap, T. Harley, D. Silver, K. Kavukcuoglu, *Asynchronous methods for deep reinforcement learning*, in: M. F. Balcan, K. Q. Weinberger (Eds.), *Proceedings of The 33rd International Conference on Machine Learning*, Vol. 48 of *Proceedings of Machine Learning Research*, PMLR, New York, New York, USA, 2016, pp. 1928–1937. URL <https://proceedings.mlr.press/v48/mniha16.html>
- [14] D. Horgan, J. Quan, D. Budden, G. Barth-Maron, M. Hessel, H. van Hasselt, D. Silver, Distributed prioritized experience replay, in: *International Conference on Learning Representations*, 2018.
- [15] Y. Du, O. Watkins, T. Darrell, P. Abbeel, D. Pathak, Auto-tuned sim-to-real transfer, in: 2021 IEEE International Conference on Robotics and Automation (ICRA), 2021, pp. 1290–1296. doi:10.1109/ICRA48506.2021.9562091.
- [16] J. Tobin, R. Fong, A. Ray, J. Schneider, W. Zaremba, P. Abbeel, Domain randomization for transferring deep neural networks from simulation to the real world, in: 2017 IEEE/RSJ International Conference on Intelligent Robots and Systems (IROS), 2017, pp. 23–30. doi:10.1109/IROS.2017.8202133.
- [17] S. Yang, K. Yu, F. Cao, H. Wang, X. Wu, Dual-representation-based autoencoder for domain adaptation, *IEEE Transactions on Cybernetics* 52 (8) (2022) 7464–7477. doi:10.1109/TCYB.2020.3040763.
- [18] W. Zhao, J. P. Queralta, T. Westerlund, Sim-to-real transfer in deep reinforcement learning for robotics: a survey, in: 2020 IEEE Symposium Series on Computational Intelligence (SSCI), 2020, pp. 737–744.
- [19] M. L. Koga, V. Freire, A. H. R. Costa, Stochastic abstract policies: Generalizing knowledge to improve reinforcement learning, *IEEE Transactions on Cybernetics* 45 (1) (2015) 77–88. doi:10.1109/TCYB.2014.2319733.
- [20] F. L. Da Silva, R. Glatt, A. H. R. Costa, Moo-mdp: An object-oriented representation for cooperative multiagent reinforcement learning, *IEEE Transactions on Cybernetics* 49 (2) (2019) 567–579. doi:10.1109/TCYB.2017.2781130.
- [21] K. Cobbe, C. Hesse, J. Hilton, J. Schulman, Leveraging procedural generation to benchmark reinforcement learning, in: *International conference on machine learning*, PMLR, 2020, pp. 2048–2056.
- [22] Z. Li, J. Xin, N. Li, End-to-end autonomous exploration for mobile robots in unknown environments through deep reinforcement learning, in: 2022 IEEE International Conference on Real-time Computing and Robotics (RCAR), IEEE, 2022, pp. 475–480.
- [23] M. Laskin, K. Lee, A. Stooke, L. Pinto, P. Abbeel, A. Srinivas, Reinforcement learning with augmented data, *Advances in neural information processing systems* 33 (2020) 19884–19895.
- [24] R. Raileanu, M. Goldstein, D. Yarats, I. Kostrikov, R. Fergus, Automatic data augmentation for generalization in reinforcement learning, *Advances in Neural Information Processing Systems* 34 (2021) 5402–5415.
- [25] K. Lee, K. Lee, J. Shin, H. Lee, *Network randomization: A simple technique for generalization in deep reinforcement learning*, in: *International Conference on Learning Representations*, 2020. URL <https://openreview.net/forum?id=HJgcvJBfVb>
- [26] K. Cobbe, O. Klimov, C. Hesse, T. Kim, J. Schulman, Quantifying generalization in reinforcement learning, in: *International Conference on Machine Learning*, PMLR, 2019, pp. 1282–1289.
- [27] N. Koenig, A. Howard, Design and use paradigms for gazebo, an open-source multi-robot simulator, in: 2004 IEEE/RSJ International Conference on Intelligent Robots and Systems (IROS)(IEEE Cat. No. 04CH37566), Vol. 3, IEEE, 2004, pp. 2149–2154.
- [28] N. H. Izadi, M. Palhang, M. Safayani, Layered relative entropy policy search, *Knowledge-Based Systems* 223 (2021) 107025.
- [29] G. Raja, S. Suresh, S. Anbalagan, A. Ganapathisubramanian, N. Kumar, Pfin: An efficient particle filter-based indoor navigation framework for uavs, *IEEE Transactions on Vehicular Technology* 70 (5) (2021) 4984–4992. doi:10.1109/TVT.2021.3072727.
- [30] F. M. Noori, D. Portugal, R. P. Rocha, M. S. Couceiro, On 3d simulators for multi-robot systems in ros: Morse or gazebo?, in: 2017 IEEE International Symposium on Safety, Security and Rescue Robotics (SSRR), 2017, pp. 19–24. doi:10.1109/SSRR.2017.8088134.
- [31] A. Ayala, F. Cruz, D. Campos, R. Rubio, B. Fernandes, R. Dazeley, A comparison of humanoid robot simulators: A quantitative approach, in: 2020 Joint IEEE 10th International Conference on Development and Learning and Epigenetic Robotics (ICDL-EpiRob), 2020, pp. 1–6. doi:10.1109/ICDL-EpiRob48136.2020.9278116.
- [32] A. Farley, J. Wang, J. A. Marshall, How to pick a mobile robot simulator: A quantitative comparison of coppeliasim, gazebo, morse and webots with a focus on accuracy of motion, *Simulation Modelling Practice and Theory* 120 (2022) 102629.
- [33] J. Weng, M. Lin, S. Huang, B. Liu, D. Makoviichuk, V. Makoviychuk, Z. Liu, Y. Song, T. Luo, Y. Jiang, Z. Xu, S. YAN, Envpool: A highly parallel reinforcement learning environment execution engine, in: *Thirty-sixth Conference on Neural Information Processing Systems Datasets and Benchmarks Track*, 2022.
- [34] H.-S. Chang, E. Learned-Miller, A. McCallum, Active bias: Training more accurate neural networks by emphasizing high variance samples, *Advances in Neural Information Processing Systems* 30 (2017).
- [35] M. G. Bellemare, Y. Naddaf, J. Veness, M. Bowling, The arcade learning environment: An evaluation platform for general agents, *Journal of Artificial Intelligence Research* 47 (2013) 253–279.
- [36] H. Van Hasselt, A. Guez, D. Silver, Deep reinforcement learning with double q-learning, in: *Proceedings of the AAAI conference on artificial intelligence*, Vol. 30, 2016.
- [37] G. Liu, W. Deng, X. Xie, L. Huang, H. Tang, Human-level control through directly trained deep spiking  $q$ -networks, *IEEE Transactions on Cybernetics* (2022) 1–12.
- [38] O. Michel, Cyberbotics Ltd. webots™: professional mobile robot simulation, *International Journal of Advanced Robotic Systems* 1 (1) (2004) 5.
- [39] J. Kulhánek, E. Derner, R. Babuška, Visual navigation in real-world indoor environments using end-to-end deep reinforcement learning, *IEEE Robotics and Automation Letters* 6 (3) (2021) 4345–4352. doi:10.1109/LRA.2021.3068106.
- [40] J. Wu, Y. Zhou, H. Yang, Z. Huang, C. Lv, Human-guided reinforcement learning with sim-to-real transfer for autonomous navigation, *IEEE Transactions on Pattern Analysis and Machine Intelligence* 45 (12) (2023) 14745–14759. doi:10.1109/TPAMI.2023.3314762.

- [41] E. Kaufmann, L. Bauersfeld, A. Loquercio, M. Müller, V. Koltun, D. Scaramuzza, Champion-level drone racing using deep reinforcement learning, *Nature* 620 (7976) (2023) 982–987.